Earthquakes and Structures, Vol. 3, No. 3-4 (2012) 473-494
DOI: http://dx.doi.org/10.12989/eas.2012.3.3.473

Rationally modeling collapse due to bending and external pressure in pipelines

André C. Nogueira*

INTECSEA, Houston, USA

(Received December 5, 2011, Revised February 22, 2012, Accepted April 10, 2012)

Abstract. The capacity of pipelines to resist collapse under external pressure and bending moment is a major aspect of deepwater pipeline design. Existing design codes present interaction equations that quantify pipeline capacities under such loadings, although reasonably accurate, are based on empirical data fitting of the bending strain, and assumed simplistic interaction with external pressure collapse. The rational model for collapse of deepwater pipelines, which are relatively thick with a diameter-to-thickness ratio less than 40, provides a unique theoretical basis since it is derived from first principles such as force equilibrium and compatibility equations. This paper presents the rational model methodology and compares predicted results and recently published full scale experimental data on the subject. Predictive capabilities of the rational model are shown to be excellent. The methodology is extended for the problem of pipeline collapse under point load, longitudinal bending and external pressure. Due to its rational derivation and excellent prediction capabilities, it is recommended that design codes adopt the rational model methodology.

Keywards: pipeline; collapse; bending; external pressure; deepwater; interaction; design

1. Introduction

The problem of pipeline collapse under external pressure and bending moment has been subject to extensive research; for example Gellin (1980), Corona and Kyriakides (1988), Zimmerman *et al*. (1995), Choi and Ayers (2005) and Wolodko and DeGeer (2006) studied this problem. Based on the dedicated research (Sintef 1996), empirical collapse equations are incorporated in DNV-OS-F101 (2010); such research used reliability based statistical analysis to best fit proposed interaction equation to test data (Collberg *et al*. 1997). API (2009) proposed a limit state design approach based largely on empirical data (Murphey and Langner 1985, Fowler and Langner 1991, Fowler 1990). The empirical approach and formulation of API (2009) and DNV-OS-F101 (2010) have withstood the test of time and usage on deepwater projects to date.

The rational model is the *first methodology* that addresses pipeline collapse from first principles of mechanics with derivable equations. This is illustrated in Figs. 1 through 9, where much of the derivations given in sections below are provided. Applications of the model are presented by comparing its predictions to experimental results and 3-dimensonal finite element analysis. As a result of this model, pipe collapse phenomenon is better understood and the influence of different

*Corresponding author, Ph.D., E-mail: Andre.Nogueira@intecsea.com

factors can be derived (e.g. ovalization, anisotropy, etc.) and incorporated in the interaction equation in a logical manner. The rational model can be extended to related problems, such as pipe collapse due to point load, as presented herein.

2. Pipe capacity and collapse mechanism

The cross sectional failure of pipelines under external pressure and longitudinal bending can be estimated using plastic hinge analysis. Collapse will occur only when four plastic hinges at 12-, 3-, 6- and 9-o'clock positions are formed in a pipe ring leading to a mechanism (Fig. 8). The maximum plastic moment capacity of the ring is calculated by adding up the plastic moment capacities of each of the hinges. This maximum plastic moment capacity of a ring is calculated based on the classical plastic analysis theory (Baker and Heyman 1969). It is assumed in the equations below that longitudinal bending compressive yield stress, σ_o, has been achieved at 6-o'clock position and also tensile yield stress has been achieved at 12-o'clock.

Plastic capacity for 3- and 9-o'clock hinges

The hinges and 3- and 9-o'clock are in the neutral axis and see no longitudinal stress (strictly speaking, on a long pipeline under plane strain Poisson's ratio will lead to longitudinal compressive stresses, however these are relatively small and will be neglect herein). See Fig. 1 for intermediate steps in the derivation of the two equations below, where the pipe thickness is t; the ring width b is taken below as L and the force ratio F/F_p is equal to σ_h/σ_o below.

- $M_p^3 = M_p^9 = M_p = L\dfrac{\sigma_o t^2}{4}$ = plastic hinge capacity without external pressure effects.
- $M_{pp}^3 = M_{pp}^9 = M_p\left[1-\left(\dfrac{\sigma_h}{\sigma_o}\right)^2\right]$ = plastic hinge capacity with compressive hoop stress σ_h due to external pressure p, where, $\sigma_h = (pOD)/(2t)$, $p_o = 2t\sigma_o/OD$, thus $p/p_o = \sigma_h/\sigma_o$.

Plastic capacity for 6-o'clock hinge under longitudinal compressive stresses

At the 6-o'clock hinge, compressive longitudinal stress lead to a bi-axial state of stress and von-Mises stress criteria is used to calculate the resulting yield stress in each plane. See Fig. 2 for some intermediate steps in the derivation of the two equations below

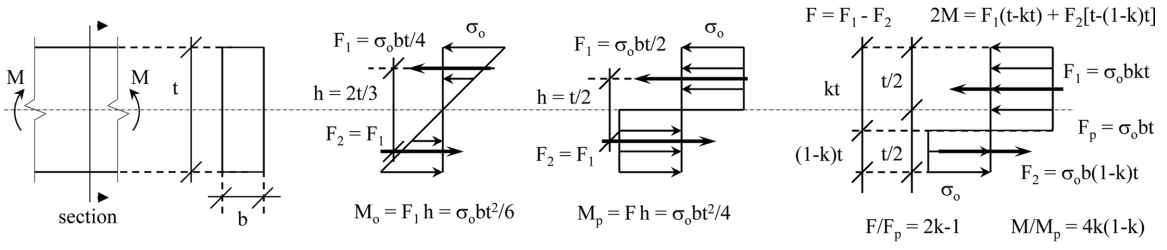

Fig. 1 Bending states of elasto-perfectly-plastic material with rectangular cross section: (a) elevation, (b) section, (c) yield, (d) fully plastic and (d) fully plastic *w*/ compressive load

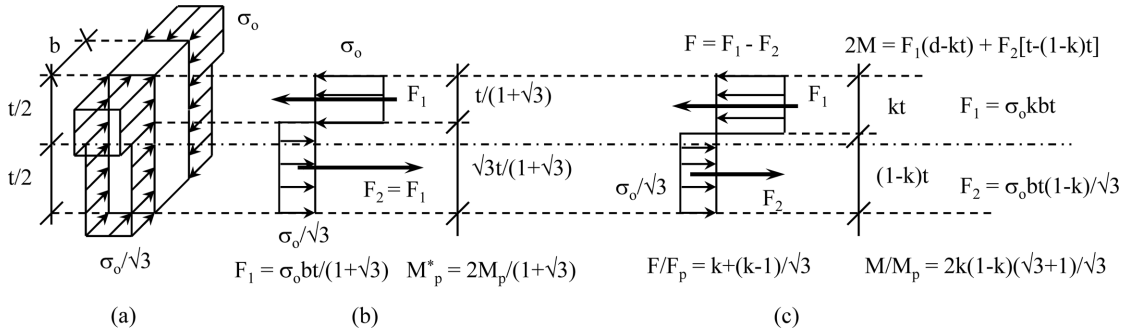

Fig. 2 Out-of-plane compression in addition to bending and bending plus axial load (elasto-plastic material *w/* rectangular cross section): (a) 3-D section, (b) fully plastic and (c) fully plastic *w/* compressive load

- $M_p^6 = M_p^* = \dfrac{2}{1+\sqrt{3}} M_p$ = plastic hinge capacity with longitudinal compressive stresses, but without external pressure induced compressive hoop stress.

- $M_{pp}^6 = M_p^*\left(\sqrt{3}\dfrac{\sigma_h}{\sigma_o}+1\right)\left(1-\dfrac{\sigma_h}{\sigma_o}\right)$ = 6-o'clock hinge capacity with longitudinal compressive stress and including compressive hoop stress due to external pressure.

Plastic capacity for 12-o'clock hinge under longitudinal tensile stresses

The plastic hinge capacities under longitudinal tensile stress are given below

- $M_p^{12} = M_p^6 = M_p^* = \dfrac{2}{1+\sqrt{3}} M_p$ = plastic hinge capacity with longitudinal tensile stresses, but without pressure induced compressive hoop stress.

- $M_{pp}^{12} = M_p^*\left(1-\sqrt{3}\dfrac{\sigma_h}{\sigma_o}\right)\left(1+\dfrac{\sigma_h}{\sigma_o}\right)$ = 12-o'clock hinge capacity with longitudinal tensile stresses and including compressive hoop stress due to external pressure.

The total bending moment capacity of a ring of pipe, $2M_{pp}^T$, is found by adding the bending moment capacity of the four hinges, and it is given in Eq. (1) below. The ring will collapse only when all four hinges are formed and the total applied static bending moment must equal $2M_{pp}^T$. For basic development of plastic collapse theory, please refer to Section 2.1 and Fig. 2.6 of Baker and Heyman (1969). The four-hinge collapse analysis has been used by Palmer and Martin (1975) in the problem of buckle propagation, but Palmer and Martin (1975) used post initial buckling energy dissipated during propagation to estimate the propagating pressure. However, herein the onset of collapse is calculated, by the equations of maximum transverse hinge capacities in a ring of a pipe

$$2M_{pp}^T = M_{pp}^3 + M_{pp}^9 + M_{pp}^6 + M_{pp}^{12} \tag{1}$$

Noting that the external pressure, p_o, that corresponds to yield stress in the hoop direction is given

by $p_o = 2t\sigma_o/OD$, thus we define the pressure ratio, P_R, as the ratio of external pressure to the yield pressure: $P_R = p/p_o = \sigma_h/\sigma_o$. Using the above formulae, thus

$$M_{pp}^T = M_p(1-P_R^2) + M_p^*(1-\sqrt{3}P_R^2) \tag{2a}$$

Or, equivalently, using the above definitions for M_p and M_p^*

$$M_{pp}^T = L\frac{\sigma_o t^2}{4}\left[(1-P_R^2) + \frac{2}{1+\sqrt{3}}(1-\sqrt{3}P_R^2)\right] \tag{2b}$$

In Eqs. (2a) and (2b), M_{pp}^T is half of the total plastic bending moment capacity of the ring of a pipe with thickness t, length equal to L, in the presence of longitudinal bending and external pressure. This bending moment capacity is transverse to the longitudinal axis of the pipeline.

In the case of longitudinal bending without external pressure, half of the total transverse plastic bending moment capacity (ring plastic capacity) is given by Eq. (3) below. How to equate the total applied bending moment with the transverse ring plastic capacity is given in the next section.

$$M_B^T = L\frac{\sigma_{oH} t^2}{4}\left(1 + \frac{2}{1+\sqrt{3}}\right) = L\frac{\sigma_{oH} t^2}{4}\sqrt{3} \tag{3}$$

3. Longitudinal bending generate transverse stress

The cornerstone of the rational model is the recognition that when a pipe is subjected to bending moment, the longitudinal stresses generate transverse stress components due to the pipe curvature. This behavior has been described qualitatively in Section 5.1 of Karamanos and Tassoulas (1991), from where Fig. 3 in this paper is taken. Such figure was the *inspiration* source for the rational model development. While Karamanos and Tassoulas (1991) provided a qualitative description of the problem of pipeline collapse (or ovalization instability) under bending, a quantitative evaluation follows.

In Fig. 4 the length of the pipe ring segment is L, the radius of curvature is ρ and the sector angle is α, thus $\rho\alpha = L$. Let dF be an infinitesimal longitudinal force vector, and let dF_v be its component

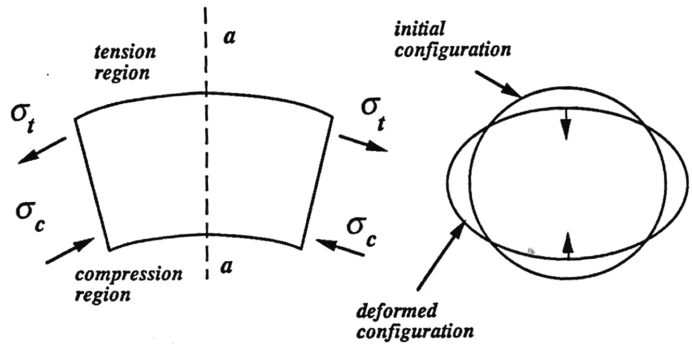

Fig. 3 Transverse stress due to longitudinal bending stresses in pipe under pure bending (source: Fig. 5.1 of Karamanos and Tassoulas (1991)

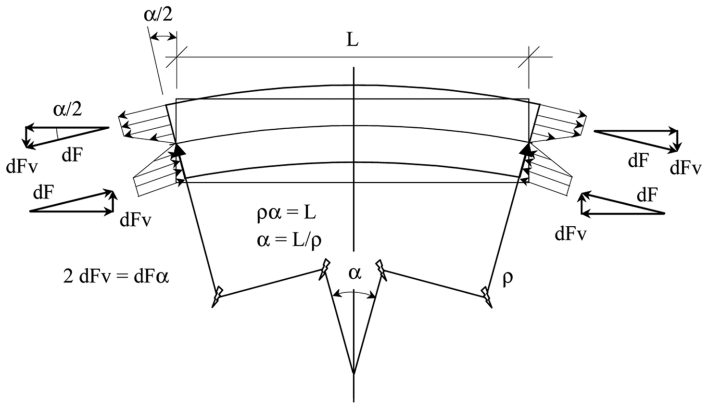

Fig. 4 Geometric relationships for longitudinal stresses in pipe under pure bending

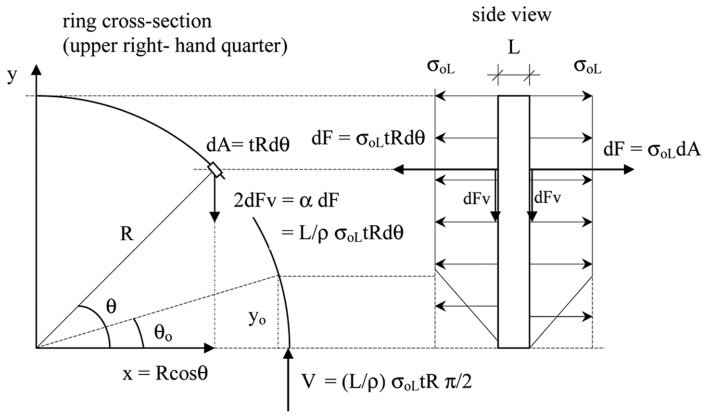

Fig. 5 Transverse loading on a pipe ring as a resulting of longitudinal bending

normal to the originally undeformed pipe axis. Similar triangles (Fig. 4) at the pipe end and assumption of a small angle lead to

$$2dF_v = \alpha dF \tag{4}$$

Fig. 5 shows a side view of the upper right-hand quarter of a ring; also shown are the stresses acting on the cross section, where for fibers distant from the neutral axis greater than y_o stresses are the longitudinal yield stress σ_{oL}. The (infinitesimal) longitudinal force is $dF = \sigma_{oL}dA = \sigma_{oL}tRd\theta$. Using these relationships, the elemental *transverse force* acting on the pipe ring is

$$2dF_v = \frac{L}{\rho}\sigma_{oL}tRd\theta \tag{5}$$

It is assumed that the entire cross section is yielding, which is fairly accurate for the strain at 12 o'clock, ε_T, greater than twice the yield strain. Integrating Eq. (5) from $\theta = 0$ to $\theta = \pi/2$, the total reaction V (see Fig. 5) at the 3 o'clock fiber is

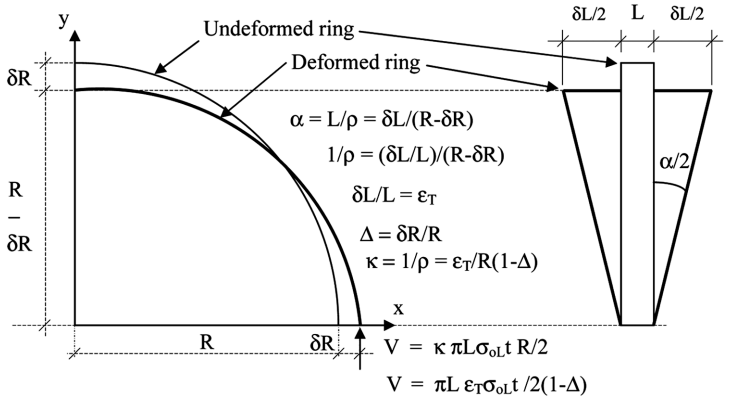

Fig. 6 Curvature-strain relationships on pipe ring under pure bending (upper right hand quarter shown)

$$V = \frac{\pi L}{2\rho}\sigma_{oL} t R \tag{6}$$

Curvature, $\kappa = 1/\rho$, and longitudinal strain can be related. Fig. 6 shows the cross section (left-side) and a side view (right-side) of the deformed and undeformed ring (upper right-hand quarter only). Ovalization effects are taken into account by the ovality ratio $\Delta = \delta R/R = \delta D/\mathrm{D}$. Simple triangle geometry shown in Fig. 6 yields the relationship between longitudinal strain at the extreme fiber, $\varepsilon_T = \delta L/L$, and curvature, $\kappa = 1/\rho$, as follows

$$\kappa = \frac{1}{\rho} = \frac{\varepsilon_T}{R(1-\Delta)} \tag{7}$$

Eqs. 6 and 7 lead to

$$V = \frac{\pi L}{2}\frac{\varepsilon_T \sigma_{oL} t}{(1-\Delta)} \tag{8}$$

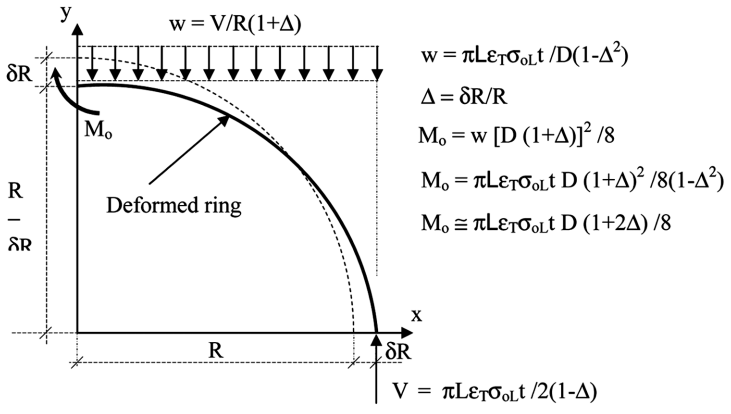

Fig. 7 Idealized uniform load on ring due to longitudinal bending and curvature

Fig. 7 shows the quarter ring cross-section. By averaging the total load across the ring span, the equivalent uniformly distributed load is $w = V/R(1 + \Delta)$ acting on the ring cross section; then using Eq. (8) the uniformly distributed load is given by

$$w = \frac{\pi L \varepsilon_T \sigma_{oL}}{(D/t)(1-\Delta^2)} \tag{9}$$

Eq. (9) is the average transverse load due to longitudinal bending on the upper half of an elasto-perfectly-plastic pipe. From elementary mechanics, the total bending moment acting on the upper half of the ring cross-section (which is treated as a simply supported beam) is $M_T = w[D(1 + \Delta)]^2/8$. Using Eq. (9) and neglecting second order ovality terms, the total moment can be written as

$$M_T = \frac{\pi L}{8} \varepsilon_T \sigma_{oL} t D(1 + 2\Delta) \tag{10}$$

Eq. (10) estimates the total transverse bending moment, due to longitudinal bending, acting on the upper half of a ring of the pipe as a function of the extreme fiber strain (see also Fig. 8). Thus, as a pipe bends, components of the longitudinal bending stresses act into the cross-section. This, in turn, generates a transverse bending moment, M_T, which ovalizes the pipe cross-section, or ring, until it fails or collapses.

4. Local buckling of pipe under pure bending

In this section, the buckling strain due to bending only is derived. Collapse happens when a cross-section ring forms a plastic hinge mechanism (four plastic hinges as indicated in Fig. 8) leading to *local buckling*. Therefore, when rings of the pipe form a mechanism, they loose their stiffness, the ovalization (initially uniform along the pipe length) will localize at the weakest point along the pipe (e.g. a thinner ring) and a local buckle will form.

Using Eq. (10), the longitudinal bending leads to a total applied moment, M_T, in the upper half of a pipe ring. Similarly, in the bottom half of a pipe ring M_T is also acting, for a total applied bending moment of (2 M_T). When this total applied moment reaches the plastic capacity of the ring, (2 M_B^T),

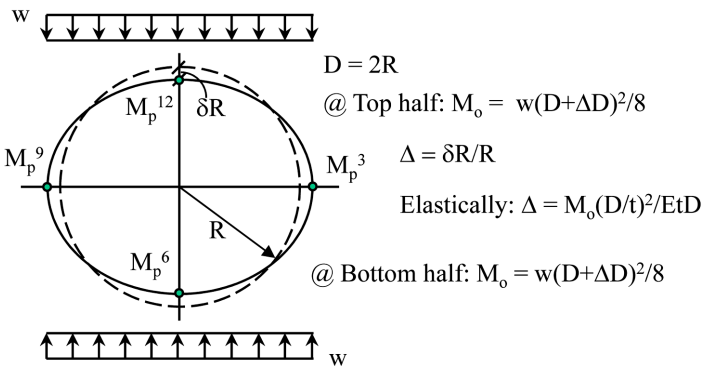

Fig. 8 Load w, total moment M_o and elastic ovality on an unit-length ring

where M_B^T is given by Eq. (3), collapse follows. The critical axial strain at 12 o'clock fiber is defined as $\varepsilon_T = \varepsilon_c$, and is found by making Eqs. (10) and (3) equal, thus

$$\frac{\pi}{8} L \varepsilon_c \sigma_{oL} t D (1 + 2\Delta) = L \frac{\sigma_{oH} t^2}{4} \sqrt{3} \tag{11}$$

The anisotropy ratio $N = \sigma_{oH}/\sigma_{oL}$ is the ratio between hoop and longitudinal yield stresses. Developing Eq. (11), and using $2\sqrt{3}/\pi \cong 1.1$, the critical axial strain at extreme (12 o'clock) fiber, ε_c, is

$$\varepsilon_c (1 + 2\Delta) = \frac{1.1N}{(D/t)} \tag{12}$$

The above equation yields the critical strains (at extreme fiber) at onset of local buckling. To solve Eq. (12), a relationship between longitudinal strain ε_T and the ovality Δ needs to be evaluated. However, a first approximation of the critical strain, denoted ε_{co}, can be found by neglecting ovalization, that is, setting $\Delta = 0$, which leads to

$$\varepsilon_{co} = \frac{2\sqrt{3}N}{\pi(D/t)} = \frac{1.1N}{(D/t)} \tag{13}$$

The above gives a first approximation of the critical buckling strain. Since it does not include ovalization effects it slightly overestimates the critical strain. Note that Eq. (13) already deduces an observed but so far unexplained feature of pipe collapse. It is clear from the derivation presented herein, that greater values of σ_{oL} (longitudinal yield stress, which generates the applied ring load) when compared to σ_{oH} (hoop yield stress, which characterizes the ring load capacity), result in a greater applied transversal load and a reduction in the ring capacity. Of course, this is captured in the anisotropy ratio N, as defined above. The ratio N can be less than one for pipe manufactured by the UOE method.

4.1 Bending strain and ovalization

In order to solve Eq. (12), a relationship between longitudinal strain at extreme fiber, ε_T, and ovalization, Δ, will be estimated as follows. Consider a unit length ring under uniformly distributed load w, such as shown in Fig. 8, in an elastic deformation mode. The elastic load-deflection for an initially perfectly circular ring of pipe is given by (Roark and Young 1982)

$$\delta R/R = \Delta = \frac{M_O (D/t)^2}{EDt} \tag{14}$$

Using $M_O = M_T$, where M_T is as given by Eq. (10) (but neglecting Δ) and substituting into Eq. (14), the following approximate relationship between longitudinal strain at the 12 o'clock fiber, ε_T, and the ovality, Δ, is obtained

$$\Delta \cong \frac{\pi}{8} \frac{\sigma_{oL}}{E} (D/t)^2 \varepsilon_T \tag{15}$$

Eq. (15) represents an initial load-deflection curve. As the longitudinal bending increases, yielding in the hoop direction starts and the load deflection starts deviating from Eq. (15). Yielding starts at the 12 o'clock fiber when the stress at the extreme fiber equals $\sigma_{oH}/\sqrt{3}$. Taking this into account and also adding an initial ovality, Δ_I, the approximate relationship between total ovality Δ, and the longitudinal strain at the 12 o'clock under bending only is given by

$$\Delta = f(\varepsilon_T) = \begin{cases} \frac{\pi}{8}\frac{\sigma_{oL}}{E}(D/t)^2\varepsilon_T + \Delta_I; \ for \ \ \varepsilon_T \le \varepsilon_{TY} \\ \Delta_Y\left[\frac{S-1}{S-(\varepsilon_T/\varepsilon_{TY})}\right]^{(S-1)}; \varepsilon_T \ge \varepsilon_{TY} \end{cases} \tag{16}$$

Where ε_{TY} and Δ_Y are given by

$$S = \varepsilon_{co}/\varepsilon_{TY} \tag{17}$$

$$\varepsilon_{TY} = \frac{8N}{3\pi\sqrt{3}(D/t)}\frac{1}{(1+2\Delta_I)} \tag{18}$$

$$\Delta_Y = \frac{N}{3\sqrt{3}}\frac{\sigma_{oL}}{E}\frac{(D/t)}{(1+2\Delta_I)} + \Delta_I \tag{19}$$

For more details on the derivation of Eqs. (16) through (19), see Nogueira and Lanan (2000).

5. Local buckling with bending and external pressure

The next step in the model development is to include the external pressure, p. If the pressure acts without bending, the elastic or elasto-plastic buckling limit state yields the critical pressure, p_c. This limit state is well known and for more details the reader is referred to Timoshenko and Gere (1961) or Fowler and Langner (1991). The API (2009) equation yields an excellent estimate of the critical pressure of a perfectly circular pipe

$$P_c = \frac{p_o p_e}{\sqrt{p_o^2 + p_e^2}} \tag{20}$$

$$p_o = \frac{2\sigma_{oH}}{(D/t)} \tag{21}$$

$$p_e = \frac{2E}{(D/t)^3(1-v^2)} \tag{22}$$

The influence of pressure in each side of Eq. (11) needs to be evaluated to determine a complete

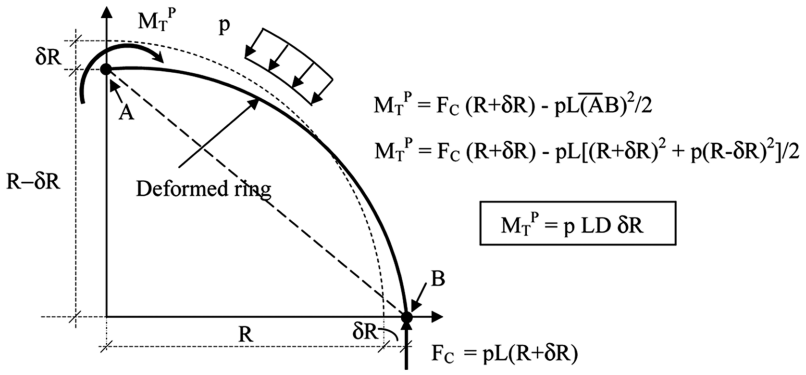

Fig. 9 Total moment due to pressure on upper half of ring

interaction equation relating bending and pressure to local buckling. The external pressure effects on the right-hand side of Eq. (11) have already been derived and Eq. (2a), which will decrease the hinge capacities.

The pressure effects on the left-hand side of Eq. (11) can be estimated by adding the total bending moment due to pressure at the 12 o'clock fiber in the deformed ring position. The total moment to be added on the left-hand side of Eq. (10) due to pressure is found developing the equation given in Fig. 9, neglecting square terms in δR; this is given in Eq. (23) below. Timoshenko and Gere (1961) provide a similar derivation in their section 7.4 and their Fig. 7-8.

$$M_T^p = pLD\delta R \tag{23}$$

Therefore, the total applied transverse bending moment in the upper half of a pipe ring due to pressure and longitudinal bending is thus, $M_A = M_T^p + M_T$. The collapse equation with the effects of external pressure is $M_A = M_{pp}^T$, as shown in Eq. (24) below.

$$DLp\delta R + \frac{\pi}{8}L\varepsilon_T\sigma_{oL}tD(1+2\Delta) = L\frac{\sigma_{oH}t^2}{4}\left[(1-P_R^2) + \frac{2}{\sqrt{3}+1}(1-\sqrt{3}P_R^2)\right] \tag{24}$$

Rearranging Eq. (24), and noting that the ring length cancels out, the collapse interaction equation relating pressure and bending effects is given by

$$\frac{8}{\pi}NP_R\Delta + \varepsilon_T(1+2\Delta) = \varepsilon_{co}\frac{\sqrt{3}-p_R^2(4-\sqrt{3})}{\sqrt{3}} \tag{25}$$

In order to use Eq. (25), the total ovality Δ as a function of longitudinal strain ε_T and pressure p, must be reasonably accurate since Eq. (25) is an equality between applied moment (left-hand side) and hinge-mechanism capacity (right-hand side), in the *ovalized (deformed)* configuration. However, $\Delta = f(\varepsilon_T)$ in Eq. (16) was derived without considerations of external pressure. It is well known that external pressure increases ovality, either initial ovality or ovality due to bending (Coronas and Kyriakides 1988). The pressure effects on the ovality is taken into account also in a rational way

following Eqs. (7-19) of Timoshenko and Gere (1961), where and initially ovalized ring has its ovality amplified by external pressure amplification ratio

$$\frac{1}{1-p/p_c} \tag{26}$$

Such a term is also used with very good accuracy estimating the elastic deflection of slender column with compressive loads, also Timoshenko and Gere (1961) Section 1.7. Therefore, the equation for ovality will take into account pressure amplification effects by using Eq. (26) as follows, where Δ is given by Eq. (16) and P_C is given by Eq. (20)

$$\Delta_{BP} = \frac{\Delta}{1-p/p_c} \tag{27}$$

Based on the above developments, the equations for the rational model are grouped in the section below for clarity and conciseness.

6. Rational model equations for pipe collapse

Interaction equation

$$\frac{8}{\pi}NP_R\Delta_{BP} + \varepsilon_T(1+2\Delta_{BP}) = \varepsilon_{co}\frac{\sqrt{3}-P_R^2(4-\sqrt{3})}{\sqrt{3}} \tag{25}$$

Normalized pressure

$$P_R = \frac{p}{p_o}$$

Total ovality

$$\Delta_{BP} = \frac{\Delta}{1-p/P_C} \tag{27}$$

Bending ovality

$$\Delta = \begin{cases} \dfrac{\pi}{8}\dfrac{\sigma_{oL}}{E}(D/t)^2\varepsilon_T + \Delta_I; \ for \ \ \varepsilon_T \le \varepsilon_{TY} \\ \Delta_Y\left[\dfrac{S-1}{S-(\varepsilon_T/\varepsilon_{TY})}\right]^{(S-1)}; \ \ \varepsilon_T \ge \varepsilon_{TY} \end{cases} \tag{16}$$

Anisotropy ratio

$$N = \frac{\sigma_{oH}}{\sigma_{oL}} \tag{17}$$

Reference strain

$$\varepsilon_{TY} = \frac{8N}{\pi 3\sqrt{3}(D/t)}\frac{1}{(1+2\Delta_I)} \tag{18}$$

Reference ovality

$$\Delta_Y = \frac{N}{3\sqrt{3}}\frac{\sigma_{oL}}{E}\frac{(D/t)}{(1+2\Delta_I)} + \Delta_I \tag{19}$$

Initial ovality

$$\Delta_I = \frac{D_{\max}-D_{\min}}{D_{\max}+D_{\min}}$$

Hyperbolic ratio $S = \varepsilon_{co}/\varepsilon_{Ty}$

Critical strain approx. $$\varepsilon_{co} = \frac{2\sqrt{3}N}{\pi(D/t)} = \frac{1.1N}{(D/t)} \tag{13}$$

Collapse pressure $$p_c = \frac{p_o p_e}{\sqrt{p_o^2 + p_e^2}} \tag{20}$$

Plastic pressure $$p_o = \frac{2\sigma_{oH}}{(D/t)} \tag{21}$$

Elastic pressure $$p_e = \frac{2E}{(D/t)^3(1-\nu^2)} \tag{22}$$

For the case of external pressure only, $\varepsilon_T = 0$ in Eq. (25). Thus, the rational model basic Eq. (25) is re-arranged as shown by Eq. (28) below, to make sure that the perfect circular pipe case is correctly represented

$$\frac{8}{\pi}NP_R\Delta_I = \varepsilon_{co}\frac{\sqrt{3} - P_R^2(4-\sqrt{3})}{\sqrt{3}}\left(1 - \frac{p}{p_c}\right) \tag{28}$$

7. Rational model comparisons

7.1 Rational model predictions vs. 3-D finite element analysis of pressure and ovalization

The effects of external pressure on pipe ovalization will be examined first. Fig. 10 reproduces Fig. 3.13 of Karamanos and Tassoulas (1993). Karamanos and Tassoulas (1993) developed a three-dimensional finite element (FE) formulation for analysis of pipes. In Fig. 10, the relationship between pressure and ovalization is shown for a pipe designated as C22J1 (pipe characteristics are shown in Fig. 11). The authors used the mean diameter to calculate a buckling pressure of $p_c = 879.6$ psi, as well as plastic pressure of $p_o = 2{,}730$ psi. Therefore, for consistency, the rational

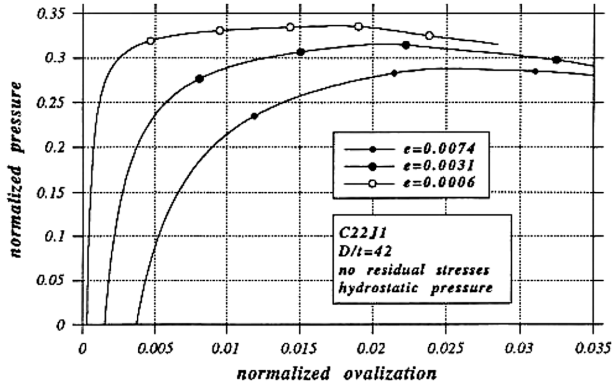

Fig. 10 Reproduction of Fig. 3.13 of Karamano and Tassooulas (1993) showing pressure (normalized by P_o) by ovalization in specimen C22J1 (see Fig. 10 below for data) obtained by three-dimensional finite-element analysis

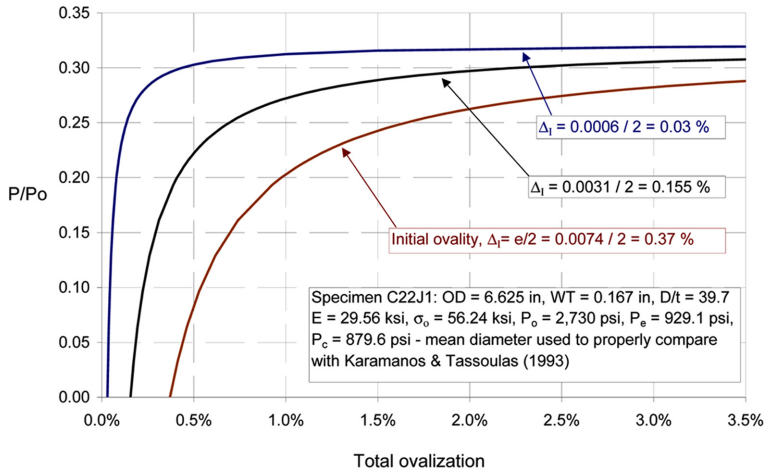

Fig. 11 Application of amplification factor given by Eq. (26) to pipe with same characteristics as specimen C22J1 with initial ovality as indicated

model predictions, shown in Fig. 9, also use the mean diameter in the relevant equations (elsewhere in this paper the outer diameter is always used). The rational model predictions shown in Fig. 11 and the FE results of Fig. 10 compare excellently.

7.2 Rational model predictions compared to experimental results of fowler (1990)

The rational model predictions are compared to experimental results presented in Table 6 of Fowler (1990). Fig. 12 shows the rational model interaction equation predictions and experimental results of Fowler (1990). It should be noted that the results for the rational model are based on the average pipe properties as shown in Fig. 12. The rational model interaction equation produces good and slightly conservative results when compared to experimental values.

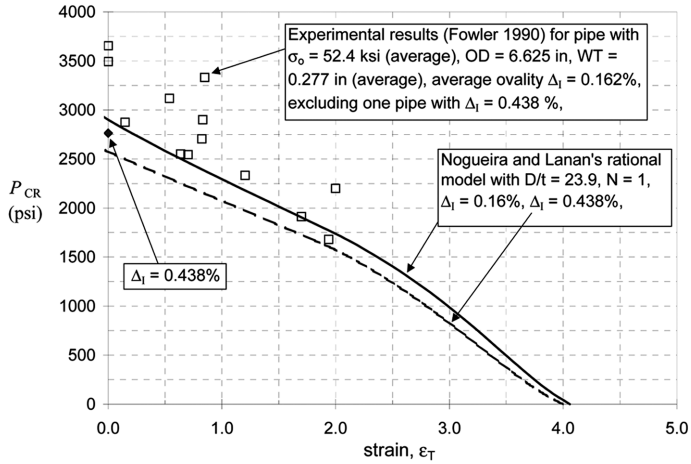

Fig. 12 Rational model pressure vs. bending strain predictions (average pipe data used) versus experimental results for pipes with $D/t = 23.9$ (average)

7.3 Rational model predictions compared to Oman to India experimental results

The rational model predictions are compared to ten experimental results of full scale collapse tests from the Oman-to-India collapse program (Stark and McKeehan 1995). This comparison is shown in Fig. 13. In this case, the individual pipe characteristics were taken into account by the rational model, including hoop and longitudinal yield data (not shown). It can be seen that excellent agreement is also obtained for almost all test results. It is noted that the hoop stress were determined by compressive tests, and for pipe specimen ZFV 18 the original data shows for this pipe a unusual low compressive hoop yield stress of 56.15 ksi, when the average hoop yield stress of 64.9 ksi for

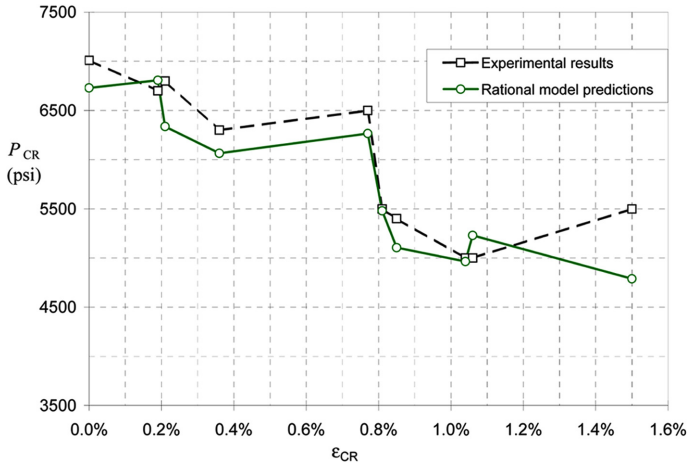

Fig. 13 Rational model prediction vs. Oman-to-India experimental results

Table 1 Test data and results for 26-inch *OD* pipes (Stark and McKeehan 1995) and rational model's predictions

Pipe designation	ZFV8	ZFV16	ZFV21	ZFV18	ZFV19	ZFV22	ZFV7	ZFV23	ZFV20	ZFV13
Experimentally applied strain (%)	0.00	0.19	0.21	0.36	0.77	0.81	0.85	1.04	1.06	1.50
Exp. collapse pressure (psi)	7,009	6,700	6,800	6,300	6,500	5,500	5,400	5,000	5,000	5,500
OD (in)	26	26	26	26	26	26	26	26	26	26
WT (in)	1.619	1.620	1.623	1.618	1.620	1.622	1.616	1.628	1.621	1.640
Δ_I(%)	0.0038	0.13	0.16	0.14	0.19	0.16	0.16	0.19	0.18	0.17
σ_{oH} (ksi)[1]	60.50	71.53	66.89	66.00	73.42	63.26	61.52	60.79	65.00	61.08
σ_{oL} (ksi)[1]	73.00	80.40	79.40	75.20	73.10	76.30	74.20	75.20	75.00	74.00
Rational model predicted collapse pressure (psi)	6730	6808	6337	6156	6266	5480	5105	4964	5230	4788
Ratio of exp. and predicted values	1.041	0.984	1.073	1.039	1.037	1.004	1.058	1.007	0.956	1.149

Note 1: Average value of measured hoop, σ_{oH} and longitudinal, σ_{oL}, yield stress for each specimen

all pipes. Such discrepancy was noted in the original collapse test program report, as probably caused by an error in the measurement of the stress-strain response, since compressive uniaxial tests are more difficult than tensile tests as they require (a) stiff testing conditions, (b) an accurately machined specimen and (c) alignment of the line of loading with the axis of the specimen. For this pipe specimen the average hoop yield stress of 64.9 ksi is used. Both Fig. 13 and in Table 1 show that excellent agreement between rational model predicted collapse pressures and the experimental collapse pressures (for the given applied strain), with the average of the ratios between prediction and experimental results is 1.035, with a standard deviation of 0.05. That is, in average, the experimental values are 3.5% higher than the predicted values, with a excellent correlation between predictions and experimental results.

7.4 Rational model predictions compared to Mardi Gras experimental results

The rational model predictions are compared to seven data points from the Mardi Gras Transportation System experimental results reported by DeGeer *et al*. (2004). Fig. 14 shows the rational model predictions and experimental results presented by DeGeer *et al*. (2004). It can be seen in Fig. 14 and in Table 2 that the rational model yields very good predictions of the experimental values. Furthermore, the ratio between experimental results and predictions is 1.141; that is, in average, the experimental values are 14.1% higher than the predicted values. It should be noted that the yield stresses used in the rational model predictions (as noted in Table 2) are not individual values reported per pipe, but average inferred by the author from Fig. 2 of DeGeer (2004), it is believed that the prediction would improve if yield stresses for each pipe were available.

7.5 Rational model predictions compared to Blue Stream experimental results

The rational model predictions are compared to fifteen data points from the Blue Stream project experimental results recently reported by DeGeer *et al*. (2005) in Fig. 15 and Table 3. The average

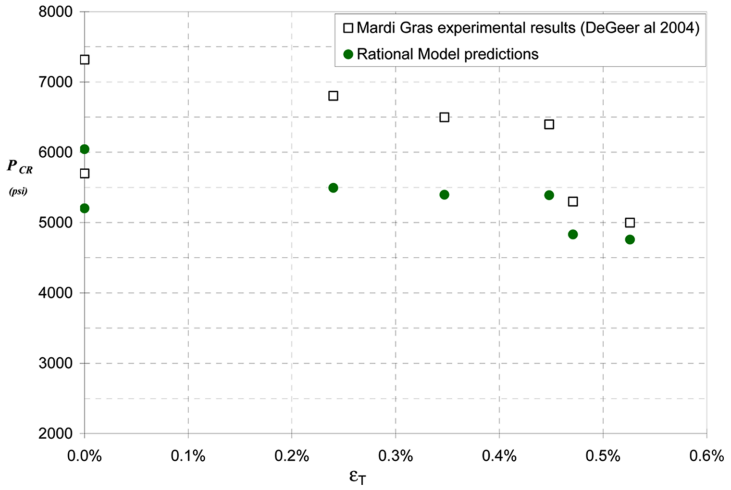

Fig. 14 Rational model prediction vs. Mardi Gras Transportation System experimental results reported by DeGeer *et al*. (2004)

Table 2 Test data and results for 28-inch *OD*, 1.5-inch *WT*, pipes (DeGeer *et al*. 2004) and rational model's predictions

Pipe designation	EP24A-HT	EP25A-AR	EP25B-HT	EP26A-AR	EP27A-AR	EP28A-HT	EP29A-HT
Experimentally applied strain (%)	0.240	0.00	0.00	0.471	0.526	0.347	0.448
Exp. Collapse pressure (psi)	6,802	5,699	7,319	5,299	4,998	6,499	6,397
OD (in)	27.982	28.001	28.009	27.988	27.979	27.973	28.001
WT (in)	1.512	1.508	1.509	1.490	1.492	1.488	1.514
Δ_f(%)[1]	0.1875	0.1775	0.0955	0.0775	0.0890	0.1175	0.1390
σ_{oH} (ksi)[2]	80.7	70.3	80.7	70.3	70.3	80.7	80.7
σ_{oL} (ksi)[2]	76.0	72.5	76.0	72.5	72.5	76.0	76.0
Rational model predicted collapse pressure (psi)	5,494	5,202	6,045	4,831	4,758	5,397	5,389
Ratio of exp. And predicted values	1.238	1.096	1.211	1.097	1.050	1.204	1.187

Note 1: Initial ovality values given are half of the those (maximum) values from Degeer *et al.* (2004) due to the difference in ovality definition.
Note 2: Average value for all pipes of measured hoop, σ_{oH} and longitudinal, σ_{oL}, yield stress for as-received (AR) and heated treated (HT) pipe as per Fig. 2 of DeGeer *et al.* (2004)

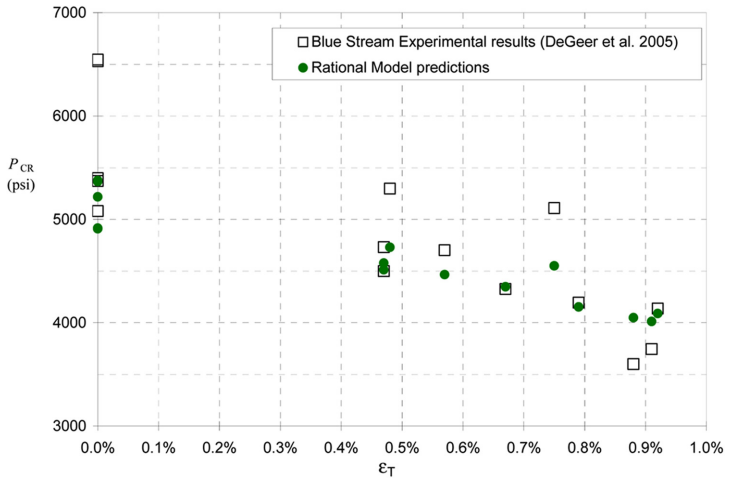

Fig. 15 Rational model prediction vs. Blue Stream experimental results - DeGeer *et al*. (2005)

of the pressure ratios between experimental results and rational model predictions is 1.05 (which means on average experimental results are 5% higher than rational model predictions), and a variance of 0.009. Thus, the rational model predictions are in excellent agreement with experimental results, and have very low dispersion. Note that for this data set the yield strength is provided for each pipe by DeGeer *et al.* (2005) in Table 3.

Table 3 Test results for Blue Stream pipe, 24-inch *OD*, 1.25-inch *WT*, Grade X65 (DeGeer *et al.* 2005) and rational model predictions

Pipe[1]	Experimental results		*OD* (in)	*WT* (in)	D_I (%)	σ_{oH} (ksi)[2]	σ_{oL} (ksi)[2]	Rational model predicted col. pressure (psi)	Ratio of exp. and predicted values
	Applied strain (%)	Collapse pressure (psi)							
1	0.000	6531	24.02	1.2488	0.221	81.97	81.57	5,376	1.21
2	0.000	6546	24.00	1.2323	0.214	80.62	80.12	5,218	1.25
3	0.478	5298	24.016	1.2465	0.214	78.99	78.23	4,729	1.12
6	0.749	5109	24.028	1.2465	0.188	80.44	80.70	4,551	1.12
7	0.000	5399	24.02	1.2480	0.184	79.75	81.86	5,365	1.01
8	0.000	5080	24.051	1.2657	0.158	67.34	73.58	4,908	1.03
9	0.000	5370	24.047	1.2469	0.192	71.30	76.92	4,916	1.09
13	0.665	4325	24.051	1.2500	0.168	72.46	75.54	4,348	0.99
14	0.918	4136	24.024	1.2500	0.240	74.85	79.39	4,089	1.01
15	0.912	3745	24.031	1.2500	0.176	70.32	74.89	4,013	0.93
16	0.786	4194	24.043	1.2575	0.187	70.72	76.34	4,153	1.01
17	0.471	4731	24.020	1.2484	0.181	74.02	77.94	4,577	1.03
18	0.469	4499	24.020	1.2469	0.190	73.15	77.21	4,512	1.00
19	0.571	4702	24.039	1.2453	0.16	73.55	77.00	4,465	1.05
20	0.876	3599	24.028	1.2480	0.269	73.98	77.43	4,049	0.89

Note 1: Pipe designation per DeGeer *et al.* (2005)
Note 2: Yield values are average for each pipe per data presented in Table 3 of DeGeer *et al.* (2005)

7.6 Rational model applied to safe point load on pipelines

Since the model is a *rational* one, it can be readily extended, for example to a pipe-to-pipe crossing condition or also to a roller load on a stinger during pipeline installation. The crossing case is examined herein. The total applied bending moment in the ring, with an applied point load at 12 o'clock (such as in a crossing situation) has three component: one due to the crossing force F, another due to the transverse stresses resulting of the longitudinal moment (Eq. (10)) and another component due to the external pressure (Eq. (23)). Fig. 16 below shows a ring of radius R which has increased its radius by δR along the 3- and 9-o'clock hinges at onset of collapse, so the total deformed ring span equals $D(1 + \Delta)$. Taking bending moments in the deformed configuration, the total applied bending moment M_T^C on the upper half of the ring due to the concentrated load F is given below by Eq. (29).

$$M_T^C = FD(1 + \Delta)/4 \tag{29}$$

The total applied transverse bending moment on the upper half of the ring due to the transverse stress w as a result of longitudinal bending (Eq. (10)), external pressure p (Eq. (23)) and point load F (Eq. (29)) is thus, $M_A = M_T^P + M_T + M_T^C$, as shown in Eq. (30) below.

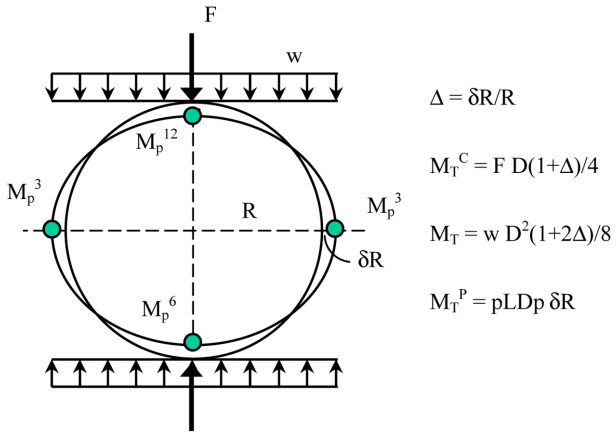

Fig. 16 Applied loads on pipe ring and the four-hinge collapse mechanism

$$M_A = FOD(1+\Delta)/4 + ODpL\,\delta R + \frac{\pi}{8}\varepsilon_T L\,\sigma_{oL} tD(1+2\Delta) \tag{30}$$

The total maximum crossing load F that causes collapse on an effective pipe ring is found as before with the rational model collapse equation $M_A = M_{pp}^T$ as developed below in Eq. (31)

$$\frac{FD(1+\Delta)}{4} + DLp\,\delta R + \frac{\pi}{8}L\,\varepsilon_T\sigma_{oL}tD(1+2\Delta) = L\frac{\sigma_{oH}t^2}{4}\left[(1+P_R^2) + \frac{2}{\sqrt{3}+1}(1-\sqrt{3}P_R^2)\right] \tag{31}$$

Eq. (31) is analogous to Eq. (24), with the addition of the bending moment due to the crossing load. The ovality function Δ is similar to Eq. (16), with the addition of the applied bending moment due to the crossing load, M_T^C, as primary bending moment; and the crossing load, F, becomes the independent variable that drives the ovalization function as well and the hyperbolic coefficient S, as follows

$$\Delta = f(\varepsilon_T) = \begin{cases} \frac{\pi}{8}\frac{\sigma_{oL}}{E}(D/t)^2\varepsilon_T + \left[\frac{(D/t)^2}{4}\times\frac{F}{EtL}\right] + \Delta_I;\ \ for\ \ F \le F_Y \\ \Delta_Y\left[\frac{S-1}{S-(F/F_Y)}\right]^{(S-1)};\ \ F \ge F_Y \end{cases} \tag{32}$$

Where F_Y is such that the ring starts yielding at 12 o'clock based on the elastic solution (neglecting the pressure effects), and Δ_Y is the corresponding ring deflection, thus

$$F_Y = \frac{tL}{3\pi(D/t)}\left(\sigma_{oH} - \frac{3\pi}{8}\varepsilon_T\sigma_{oL}(D/t)\right) \tag{33}$$

$$\Delta_Y = \frac{\pi}{8}\frac{\sigma_{oL}}{E}(D/t)^2\varepsilon_T + \left[\frac{(D/t)^2}{4}\times\frac{F_Y}{EtL}\right] + \Delta_I \tag{34}$$

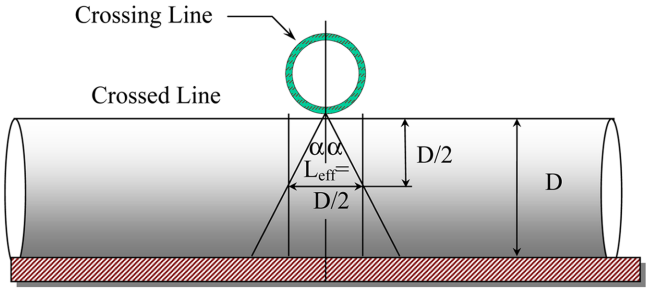

Fig. 17 Effective ring length in pipeline under point load or direct contact

$$S = F_o / F_Y \tag{35}$$

Where F_o is such that the ring collapses under external pressure, neglecting axial bending (for simplicity), thus

$$F_o = \frac{(M_{pp}^{12} + M_{pp}^{3})D}{4} \tag{36}$$

Finally, in order to have a completely defined equation, the effective ring length is conservatively defined as half of the outside diameter, as given by Eq. (36) below. This definition corresponds to a load spread angle of $\alpha \cong 26.5^{o}$ (see Fig. 17).

$$L = L_{eff} = OD/2 \tag{37}$$

To illustrate the methodology for calculation the maximum crossing load on pipelines per the rational model equations 31 through 36, Table 4 below is presented. Numerical results for all variables are given for several pipeline parameters. The table is broken in three parts for easy of reading. Basic input data are: pipeline yield stress = 65 ksi, water depth = 4,400 ft, thus external water pressure = 1,956 psi, initial ovalization for all pipes = 1%, the maximum longitudinal bending moment for each pipe is assumed (should be calculated based on a global bending analysis), for

Table 4 Sample calculations for maximum point load for several pipelines under pressure and bending-rational model parameters given

OD	*WT*	*D/t*	Effective ring length		Hoop stress	Hoop stress to hoop yield ratio	Maximum longitudinal bending moment at crossing location	*po*	*pe*	*pc* (ksi)	Pipe moment of inertia	Maximum longitudinal stress	Maximum longitudinal strain
(inch)	(inch)	-	(*L*/*OD*)	*L* (inch)	(ksi)	(*s*/so)	(kip-ft)	(ksi)	(ksi)	(ksi)	inch^4	(ksi)	inch/inch
6.625	**0.625**	10.60	**0.50**	3.31	10.4	0.159	**25.000**	12.3	53.5	12.0	53	18.74	0.00065
8.625	**1.000**	8.63	**0.50**	4.31	8.4	0.130	**70.000**	15.1	99.3	14.90	174	20.81	0.00072
10.75	**1.000**	10.75	**0.50**	5.38	10.5	0.162	**60.000**	12.1	51.3	11.77	364	10.63	0.00037
12.75	**0.750**	17.00	**0.50**	6.38	16.6	0.256	**50.000**	7.6	13.0	6.6	509	7.52	0.00026
20	**1.125**	17.78	**0.50**	10.00	17.4	0.267	**200.000**	7.3	11.3	6.15	2971	8.08	0.00028

Table 4 Continued

Crossing load that leads to ring start yielding, *Fy*	Maximum crossing load - calculated by macro	Total ovalization ratio				Applied moment on ring due to crossing load	Applied moment on ring due to external water pressure	Applied moment on ring due to longitudinal bending	Total moment applied on ring
		Δ (Elastic)	Δ*y*	Estimated ovalization *w/o* pressure	Total ovalization				
Kips	(kips)	(*dR*/*R* = *dD*/*D*)	(inch/inch)	(inch/inch)	(inch/inch)	(kip-inch)	(kip-inch)	(kip-inch)	(kip-inch)
13.187	17.51	1.825%	1.623%	2.917%	3.488%	30.01	4.96	0.24208	35.2
33.786	47.45	1.710%	1.507%	3.269%	3.763%	106.17	11.80	0.73249	118.7
33.876	44.75	1.833%	1.632%	2.896%	3.473%	124.43	21.09	0.57832	146.1
19.045	19.15	2.005%	1.999%	2.016%	2.867%	62.80	29.06	0.42639	92.3
42.823	40.30	1.984%	2.045%	1.984%	2.910%	207.37	113.80	1.69301	322.9

Table 4 Continued

Mp - average of 3 & 9 o'clock		*Mp* - average of 12 & 6 o'clock		*MP* - average all hinges	Maxium crossing force		Hiperbolic coefficient
No external pressure	With external pressure	No external pressure	With external pressure	With external pressure	Wihtout pressure or bending effects, *Fo*	With pressure or bending effects, *Fx*	*S* = *Fo*/*Fy*
(kip-inch)	(kip-inch)	(kip-inch)	(kip-inch)	(kip-inch)	(kips)	(kips)	
21.0	20.5	15.4	14.7	35.2	21.3	**17.5**	1.6119
70.1	68.9	51.30	49.8	118.7	55.1	**47.5**	1.6294
87.3	85.1	63.94	61.0	146.1	54.4	**44.7**	1.6048
58.3	54.5	42.7	37.8	92.3	29.0	**19.2**	1.5202
205.7	191.0	150.56	131.9	322.9	64.6	**40.3**	1.5079

example it equals 25 kip-ft for the 6-inch pipeline. Please note that such table is the result of an excel spreadsheet where the maximum crossing load is found by making the total moment applied on the ring, equal to the average plastic moment (*Mp*) capacity for all rings. Please note that the maximum crossing load given below is an ultimate type load, and appropriate safety coefficients should be applied for a safe design load. A factor of safety of 1.5 is suggested.

8. Conclusions

A rational model for ultimate pipe strength under pressure and bending was derived from first principles. With the rational model the pipe collapse phenomenon is better understood and the influences of different terms (e.g. ovalization and anisotropy) are incorporated by derivation. Published full scale test results are compared to the rational model predictions and excellent agreement is obtained. The model is extended to that of a pipe-to-pipe contact crossing and similarly could be easily extended to model (a) local buckling potential due to roller loads on a *S*-lay stinger configuration, (b) local buckling of a buried pipeline subjected to relatively high longitudinal bending without external pressure. Note that case (a) is of importance on laying pipe in deepwater subject to relatively high roller loads and (b) is of importance when assessing if a buried pipeline can withstand large fault deformation and not locally buckle (Paolucci *et al*. 2010). It is

recommended that independent evaluation of the rational methodology is done, along with finite element analysis and test results, to assist in improving the equations used in existing codes.

References

API RP1111 (2009), *Design, construction, operation, and maintenance of offshore hydrocarbon pipelines (Limit state design)*, American Petroleum Institute, Washington, D.C.

Baker, J. and Heyman, J. (1969), *Plastic design of frames*, Cambridge University Press, Cambridge, Great Britain.

Choi, H.S. and Ayers, T.R. (2005). "Pipeline collapse methodology for ultra deepwater," *ASME Offshore Mech. Arct. Eng., Conf.* (OMAE), Halkidiki, Greece.

Colberg, L., Mork, J.K. and Bjornsen, T. (1997), "DNV'96: Application of a limit state based design", *Offshore Mech. Arct. Eng*., **5**, 109-117.

Corona, E. and Kyriakides, S. (1988), "On the collapse of inelastic tubes under combined bending and pressure", *Int. J. Solid. Struct*., **24**(5), 505-535.

DeGeer, D., Marewski, U., Hillenbrand, H.G., Weber, B. and Crawford, M. (2004), "Collapse testing of thermally treated line pipe for ultra-deepwater applications", *Proceedings of 23rd, Offshore Mech. Arct. Eng*. (OMAE), Vancouver, Britsh Columbia, Canada.

DeGeer, D., Timms, C. and Lobanov, V. (2005), "Blue stream collapse test program", *Proceedings of 24rd, Offshore Mech. Arct. Eng*. (OMAE), Halkidiki, Greece.

DNV-OS-F101 (2010), *Submarine pipeline systems*, Det Norske Veritas, Norway.

Fowler, J.R. (1990), "Large scale collapse testing", *Proceedings of Collapse of Offshore Pipelines*, Pipeline research Committee - American Gas Association, Houston, Texas.

Fowler, J.R. and Langner, C.G. (1991), "Performance limits for deepwater pipelines", *Offshore Tech. Conf*., Paper 6757.

Gellin, S. (1980), "Plastic buckling of long cylindrical shells under pure bending", *Int. J. Solid. Struct*., **16**(5), 397-407.

Karamanos, S.A. and Tassoulas, J.L (1991), "Stability of deep-water pipelines under combined loading", *Offshore Tech. Res. Center*, Report No. 6/91-B-18-100, College Station, Texas.

Karamanos, S.A. and Tassoulas, J.L (1993), "Stability of tubes under external pressure and structural loading," *Offshore Tech. Res. Center*, Report No. 11/93-B51100, College Station, TX.

Murphey, C. and Langner, C. (1985), "Ultimate pipe strength under bending, collapse and fatigue", *ASME Offshore Mech. Arct. Eng*., *Conf*. (OMAE).

Nogueira, A.C. and Lanan, G.A. (2000), "Rational modeling of ultimate pipe strength under bending and external pressure", *Int. Pipeline Conf*., Calgary, Canada.

Palmer, A.C. and Martin, J.H. (1975), "Buckle propagation in submarine pipelines", *Nature*, **254**, 46-48.

Paolucci, R., Griffini, S. and Mariani, S. (2010), "Simplified modeling od continuums buried pipelines subject to earthquake fault rupture", *Earthq. Struct*., **1**(3), 253-267.

Roark, J.R. and Young, W.C. (1982), *Formulas for stress and strain*, 5th Ed., McGraw-Hill, NY, New York.

Sintef (1996), "Superb project: Buckling and collapse limit state", Sintef, Trondheim, Norway.

Stark, P.R. and McKeehan, D.S. (1995), "Hydrostatic collapse research in support of the Oman India gas pipeline", *Offshore Tech. Conf*., Paper 7705.

Timoshenko, S.P. and Gere, J.M. (1961), *Theory of elastic stability*, McGraw-Hill, NY.

Wolodko, J. and DeGeer, D. (2006), "Critical local buckling conditions for deepwater pipelines", *ASME Offshore Mech. Arct. Eng*., *Conf.* (OMAE), Hamburg, Germany.

Zimmerman, T.J.E., Stephens, M.J., DeGeer, D.D. and Chen, Q. (1995), "Compressive strain limits for buried pipelines", *ASME Offshore Mech. Arct. Eng. Conf*., **5**, 365-378.

SA

Nomenclature

E = Young's modulus
F_p = plastic force
F_o = 12 o'clock point force on a ring under external pressure that leads to plastic collapse
L = ring length; length of a pipe segment
M = bending moment
M_o = yield moment
$M_B{}^T$ = total moment acting on a unit-length ring of pipe under bending only
M_p = plastic moment under uniaxial stress
M_p^* = plastic moment under biaxial stress
M_p^3 = 3 o'clock plastic hinge capacity without external pressure effects
$M_{pp}{}^3$ = 3 o'clock plastic hinge capacity with external pressure effects
$M_{pp}{}^T$ = half of total plastic hinge capacity of a pipe ring with bending and pressure effects
N = σ_{oH}/σ_{oL}
p = external pressure on a pipe
p_o = yield load pressure (or plastic pressure) on a pipe
p_c = collapse pressure on a pipe
p_e = elastic collapse pressure on a pipe
t = pipe wall thickness
R = pipe radius
V_{ur} = total reaction at 3 o'clock fiber in a unit-length ring of pipe under bending
w = uniformly distributed load
α = sector angle of pipe segment with length L
δR = change in radius of pipe cross-section (Fig. 3)
δD = 2 δR
Δ = $\delta R/R$ = ovality
Δ_{BP} = Δ due to bending and pressure
Δ_{yo} = Δ at onset of yield in the hoop direction of pipe under bending
Δ_I = Initial ovality on a pipe
ε_{co} = critical longitudinal pipe strain at extreme fiber neglecting ovalization effects
ε_T = (critical) longitudinal pipe strain at extreme fiber, $\varepsilon_T = \varepsilon_c$ at onset of local buckling
ε_{Ty} = longitudinal pipe strain at extreme fiber at onset of yielding
ε_{Tyo} = longitudinal pipe strain at extreme fiber at onset of yielding neglecting ovalization
σ_o = yield stress
σ_{oL} = yield stress in longitudinal pipe direction
σ_{oH} = yield stress in transverse (hoop) pipe direction
ρ = radius of curvature
κ = $1/\rho$ = curvature